ornl

ORNL/TM-7283

OAK RIDGE NATIONAL LABORATORY

UNION CARBIDE

An Ion Energy Recovery Experiment Based on Magnetic Electron Suppression

J. Kim
W. L. Stirling
W. K. Dagenhart
G. C. Barber
N. S. Ponte

OPERATED BY
UNION CARBIDE CORPORATION
FOR THE UNITED STATES
DEPARTMENT OF ENERGY

ORNL/TM-7283
Dist. Category UC-20

Contract No. W-7405-eng-26

FUSION ENERGY DIVISION

AN ION ENERGY RECOVERY EXPERIMENT BASED ON MAGNETIC ELECTRON SUPPRESSION

J. Kim, W. L. Stirling, W. K. Dagenhart,
G. C. Barber, and N. S. Ponte

Date Published - May 1980

NOTICE This document contains information of a preliminary nature. It is subject to revision or correction and therefore does not represent a final report.

Prepared by the
OAK RIDGE NATIONAL LABORATORY
Oak Ridge, Tennessee 37830
operated by
UNION CARBIDE CORPORATION
for the
DEPARTMENT OF ENERGY

CONTENTS

ABSTRACT

We present results of a proof-of-principle experiment on direct recovery of residual hydrogen ions based on a magnetic electron suppression scheme. Ions extracted from a source plasma a few kilovolts above the ground potential (∿20 A) are accelerated to 40 keV by a negative potential maintained on a neutralizer gas cell. As the residual ions exit the gas cell, they are deflected from the neutral beam by a magnetic field that also suppresses gas cell electrons and then recovered on a ground-potential surface. Under optimum conditions, a recovery efficiency (the ratio of the net recovered current to the available full-energy ion current) of 80% ± 20% has been obtained. Magnetic suppression of the beam plasma electrons was rather easily achieved; however, handling the fractional-energy ions originating from molecular species (H_2^+ and H_3^+) proved to be extremely important to recovery efficiency.

1. INTRODUCTION

When charge exchange is used, ion-to-neutral conversion efficiency decreases rapidly as the energy per nucleon increases. Because of this, neutral injectors based on positive ions appear less attractive for future fusion reactors that require deuterium beams of up to 200 keV. One way to improve the injector efficiency is to recover the residual ion energy that otherwise would be wasted. Efforts aimed at direct recovery of charged particle energy began with the concept of recovering the energy of end-lost ions in magnetic mirror devices.[1,2] The main difficulty in a direct recovery device is to effectively prevent the space-charge neutralizing electrons from flowing along with the ions as the ions are decelerated. Both electrostatic[3-6] and magnetic[7,8] suppression schemes have been tried on neutral beam test stands.

We previously reported a preliminary result of the magnetic blocking experiment,[7] which provided evidence of successful electron blocking by a transverse magnetic field. In this paper, we describe a follow-up experiment that incorporated a modified recovery geometry and improved diagnostics. The geometry of the gas cell extension used in this experiment precludes any strong electric fields in the region where ions are bent by the magnetic field. This geometry may be termed *loosely coupled*, in contrast to the previous geometry,[7] in which the ground-potential surface is rather closely coupled to the gas cell end in the region of magnetic deflection. The typical beam current and energy for the experiment reported here were 20 A and 35 keV, respectively, at the acclerator column. The residual full-energy ion current available at the end of the gas cell was about 10% of the total extracted current.

2. EXPERIMENTAL CONFIGURATION AND DIAGNOSTICS

The ISX-B prototype beam line[9] was modified to be suitable for direct ion energy recovery experiments. A schematic of the experiment is shown in Fig. 1 along with the potential distribution along the beam line. In this experiment, the existing charged-particle separation magnet is used as an electron suppressor, with the neutralizer gas cell extended to the magnet, and the power supplies are connected so as to maintain a high negative electrostatic potential on the gas cell structure while the ion source and the recovery plate are near or at ground potential. As shown in Fig. 1, a series of resistive loads across the high-voltage power supply provides proper voltages to the electrodes, namely, the decel voltage across the second gap and the electron collector voltage of a few kilovolts (positive with respect to the gas cell potential). A separate power supply is used to keep the ion source plasma slightly positive above ground so that the recovered ions come to the ground plate with a finite kinetic energy. Molecular ions (H_2^+ and H_3^+), extracted from the source along with atomic ions (H_1^+), are dissociated into atomic particles as they pass through a near-equilibrium gas cell. These particles have energies of one-half (E/2) or one-third (E/3) the original acceleration energy (E) and cannot reach the ground-potential surfaces.

The geometry of the gas cell extension is shown in Fig. 2. The end structure is a metal box with its forward (downstream) sides open for the passage of neutrals and deflected full-energy ions. An electron collector ring is fastened around the opening of the box and extends a few centimeters beyond it. The side plates of the extension overlap

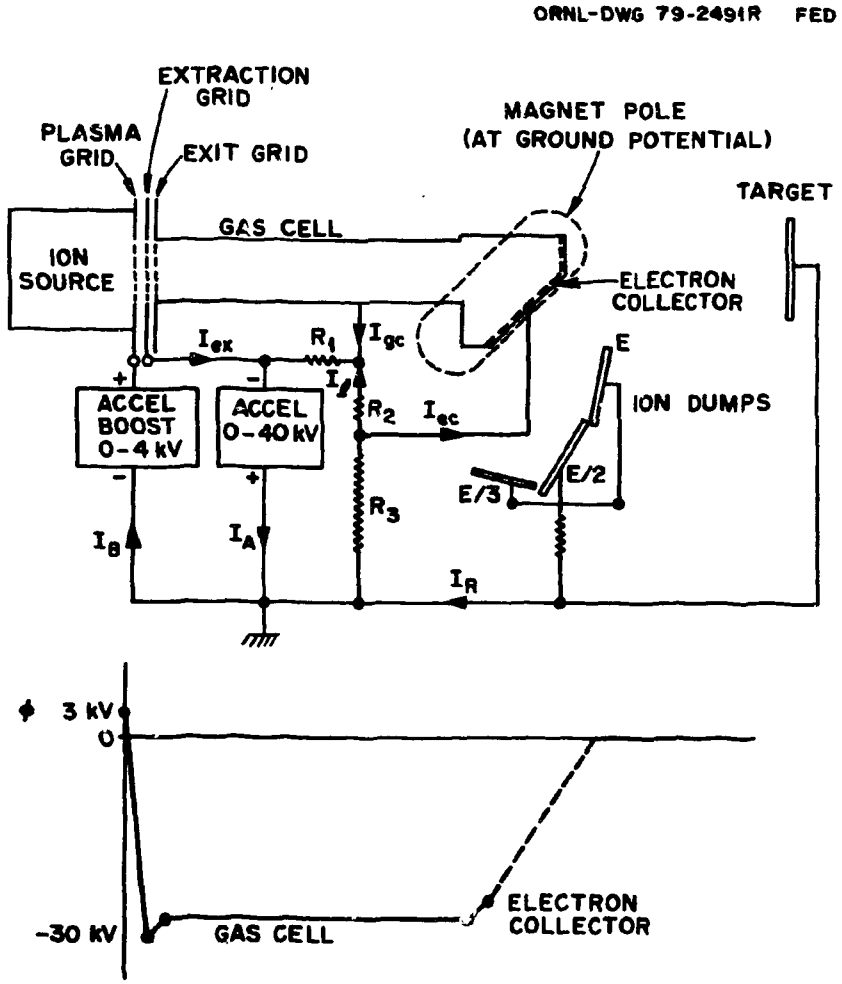

Fig. 1. Schematic of ion recovery experiment and the potential distribution along the beam line.

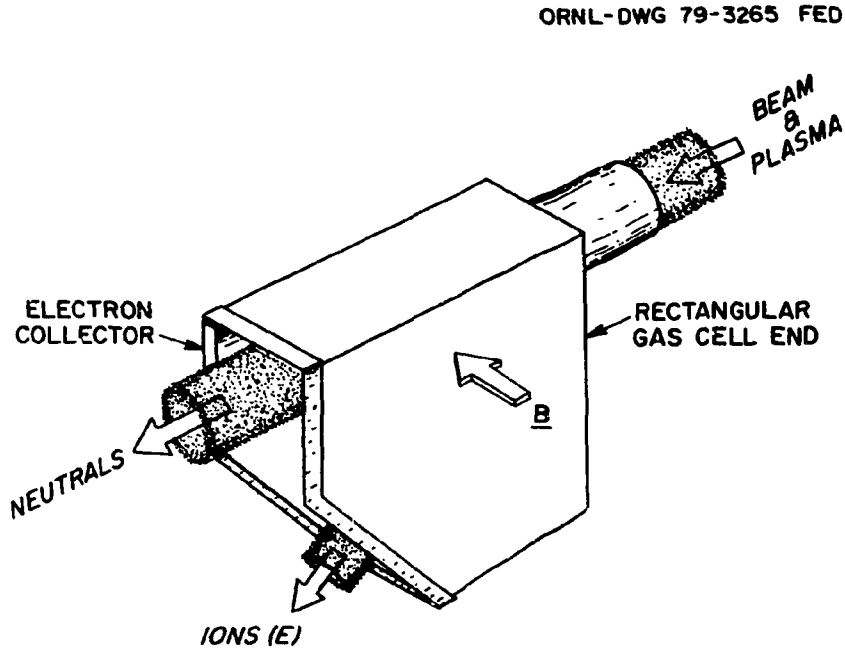

Fig. 2. Geometry of the end section of the gas cell.

essentially all of the magnet pole face. With this geometry, both the electrons and residual ions experience the transverse magnetic field in the absence of any strong electric fields. The field strength of the transverse magnet is approximately Gaussian in the direction parallel to the pole face (an e-folding length of ±17 cm) and scales linearly with the coil current (the midplane field strength of 3.5×10^{-4} T/A).

The separation of the beam plasma electrons and the residual energetic ions begins at the entrance to the magnet region; there, electrons tend to gyrate along the transverse flux lines, whereas ion trajectories are only bent. Any electric fields owing to the ions moving away or to field penetration through the open end are approximately perpendicular to the magnetic field, producing only $\underline{E} \times \underline{B}$ drifts of the electrons. It is expected that the beam plasma electrons eventually terminate either on the gas cell wall or at the collector ring. Under a proper range of magnetic field strengths, the lower-energy ions (E/2 and E/3) are reflected into the inside walls of the gas cell, whereas the full-energy ions are deflected from the neutral beam passage and leave the gas cell. The full-energy ions then reach the surrounding ground- potential surfaces while being decelerated.

Two diagnostic techniques were employed in the experiment: calorimetry and current measurement. The essential places in the beam line were calorimetrically monitored by measuring the temperature rise of cooling water to determine beam power depositions. The total power accountability was about 90% of the accelerator power under the non-recovery mode of operation. Measured currents include those through the booster supply (I_B), through the accelerator power supply (I_A), from the

extraction grid (I_{ex}), from the gas cell (I_g), and from the electron collector (I_{ec}) (see Fig. 1). The booster current I_B represents the total system current, which comprises the total extracted ion current from the discharge source plasma and the small parasitic current in the accelerator column. If any net recovery of ions is made, then the drain current through the accelerator supply solely attributable to the beam will be smaller than I_B, where the drain current I_D is obtained from the measured I_A by subtracting the leakage current I_ℓ through the resistive load in our present circuitry. The net recovered ion current I_R is therefore estimated as $I_R = I_B - I_D$. This current and the corresponding power $I_R V_g$, where V_g is the gas cell voltage, are simply unused (or saved) in the accelerator supply in the recovery scheme of Fig. 1. Here I_ℓ and I_{ec} are the sources of energy loss, which can be made negligible in actual application. Both the decel gap potential and the electron collector potential can be supplied by separate power supplies of a few kilovolts floating at the high negative potential.

3. EXPERIMENTAL RESULTS

The experimental data are analyzed in terms of current recovery efficiency, which is defined as the ratio of the net recovered ion current to the available full-energy ion current at the end of the gas cell. This can be expressed as

$$\eta_{IR} = \frac{I_B - I_D}{I_B \eta_g f_1 f_+^\infty} \quad , \tag{1}$$

where η_g is the total beam transmission efficiency through the gas cell, f_1 is the fraction of atomic species (e.g., H_1^+ or D_1^+) in the extracted beam, and f_+^∞ is the equilibrium fraction of ions in the neutralizer gas cell (e.g., H_2 or D_2 gas).

The overall injector system efficiency *with* ion energy recovery (η^R) is expressed as the ratio of the neutral beam energy delivered to the target (i.e., fusion plasmas) to the total consumed energy, or

$$\eta^R = \frac{I_B V_T f_o^\infty \eta_t}{I_B V_T - I_B (V_T - V_B) f_+^\infty \eta_g f_1 \eta_{IR} + I_{ec} V_{ec}} \quad , \tag{2}$$

where V_T, V_B, V_{ec}, f_o^∞, and η_t respectively are the total accelerator voltage, the boost voltage, the electron collector bias with respect to the gas cell potential, the equilibrium fraction of neutrals, and the transmission efficiency to the target. The energy loss term owing to electron current drain to the collector ($I_{ec} V_{ec}$) is (or can be made)

negligible in practice compared with the recovered energy term. The ratio of the electron current to the residual ion current is on the order of $(m_i E_e / m_e E_i)^{1/2}$, which is typically less than 1 ($E_e \sim$ a few eV, $E_i \sim$ tens of keV, and $m_i/m_e \sim$ 1838-3677), and $V_{ec}/V_T \ll 1$. If we neglect the electron energy loss term and if we let $f_+^\infty = 1 - f_o^\infty$ and $V_B/V_T = 0.03$ as a practical value, then Eq. (2) simplifies to

$$\eta^R = \frac{f_o^\infty \eta_t}{1 - 0.97(1 - f_o^\infty)\eta_g \eta_{IR} f_1} . \tag{3}$$

Note that the numerator in this equation is the system efficiency *without* the recovery of ion energy.

Current recovery efficiencies are plotted in Fig. 3 as a function of the magnetic field strength for different energies of hydrogen ion beams. Typically, $f_1 \cong 0.85$ and $\eta_g \cong 0.43$, and thus the available full-energy ion current is about 10% of I_B. There exists a critical field strength below which the current recovery efficiency η_{IR} becomes negative, that is, there is more electron drain current than recovered ion current. The critical magnetic field strength seems to increase with the increased beam energy. This seems to indicate that recovery is predominantly spoiled by fractional-energy ions that leak out of the end of the gas cell and turn back to the outside walls of the cell, generating secondary electrons. The secondary electrons then freely accelerate onto the ground-potential surfaces, canceling the recovered positive ion current. As the magnetic field strength is increased, the orbits of the fractional-energy ions become tighter, and hence fewer lower-energy ions

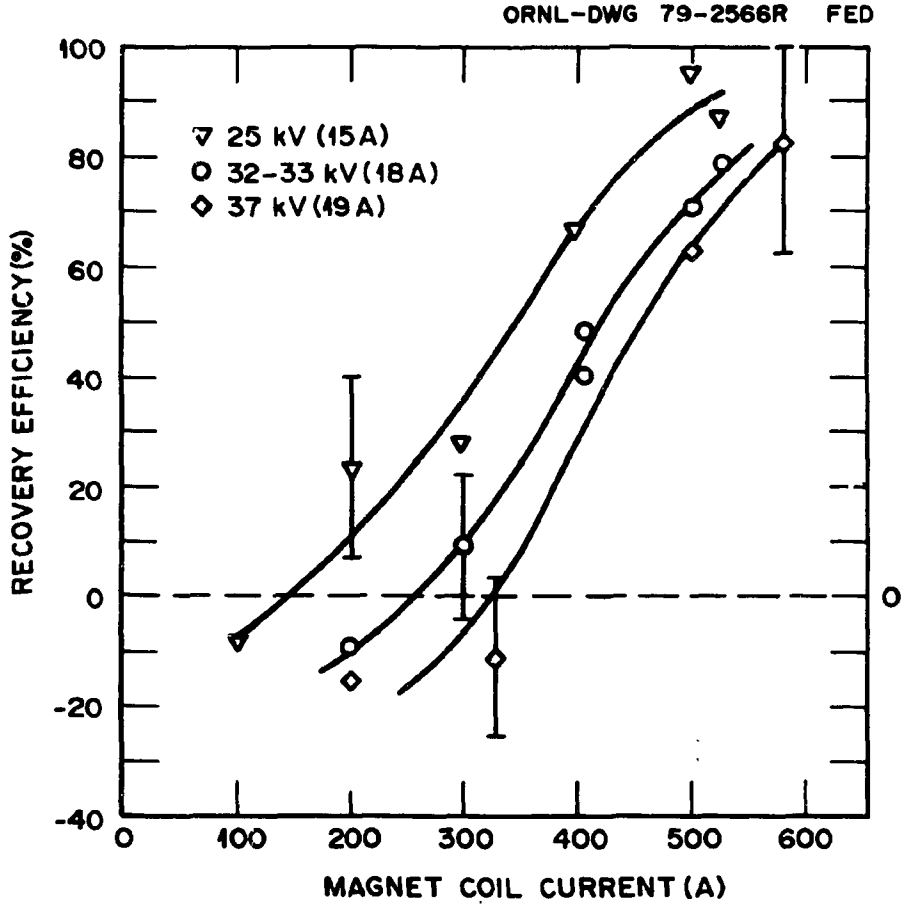

Fig. 3. Current recovery efficiency data as a function of magnetic field strength for three beam energies.

leak out. This conjecture is partly supported by the monotonic increase of η_{IR} as the magnetic field strength increases, because the effectiveness of electron suppression is *not* believed to be such a smooth function of the magnetic field strength. Because of the limited magnet coil power supply, however, we were not able to verify a plateau at the high-efficiency region. Despite the large error bars associated with both measurements and analyses, it is fair to conclude from the data shown in Fig. 3 that $\eta_{IR} = 80\% \pm 20\%$ is achievable.

Calorimetric measurements of beam power deposition show an independent verification of the performance of ion energy recovery. The top portion of Fig. 4 is a collection of data as a function of field strength that shows that the total sum of calorimetrically measured powers normalized to $I_B V$ decreases, or the unaccounted power increases, as the recovery efficiency increases. We have noted that the calorimetry system has a 90% accountability in the *nonrecovery* mode of operation. At high magnetic fields where $\eta_{IR} \cong 80\%$ is obtained from measurements of currents, a net power of 8% of $I_B V_T$ (i.e., 18% minus 10%) is "missing," or saved, under the recovery mode. In other words, calorimetric measurements showed that about 8% of I_B was recovered, which is consistent with the result from the current measurement ($I_R \approx$ 6-10% of I_B).

Variations of power loading to two places of interest are examined as a function of magnetic field in the bottom portion of Fig. 4. Contributions to power loading on the electron collector ring are from direct interception of deflected ions (mainly on the bottom portion of the ring) and from collected electrons being accelerated to V_{ec} (mainly on the top portion of the ring). Data plotted in Fig. 4 show a somewhat

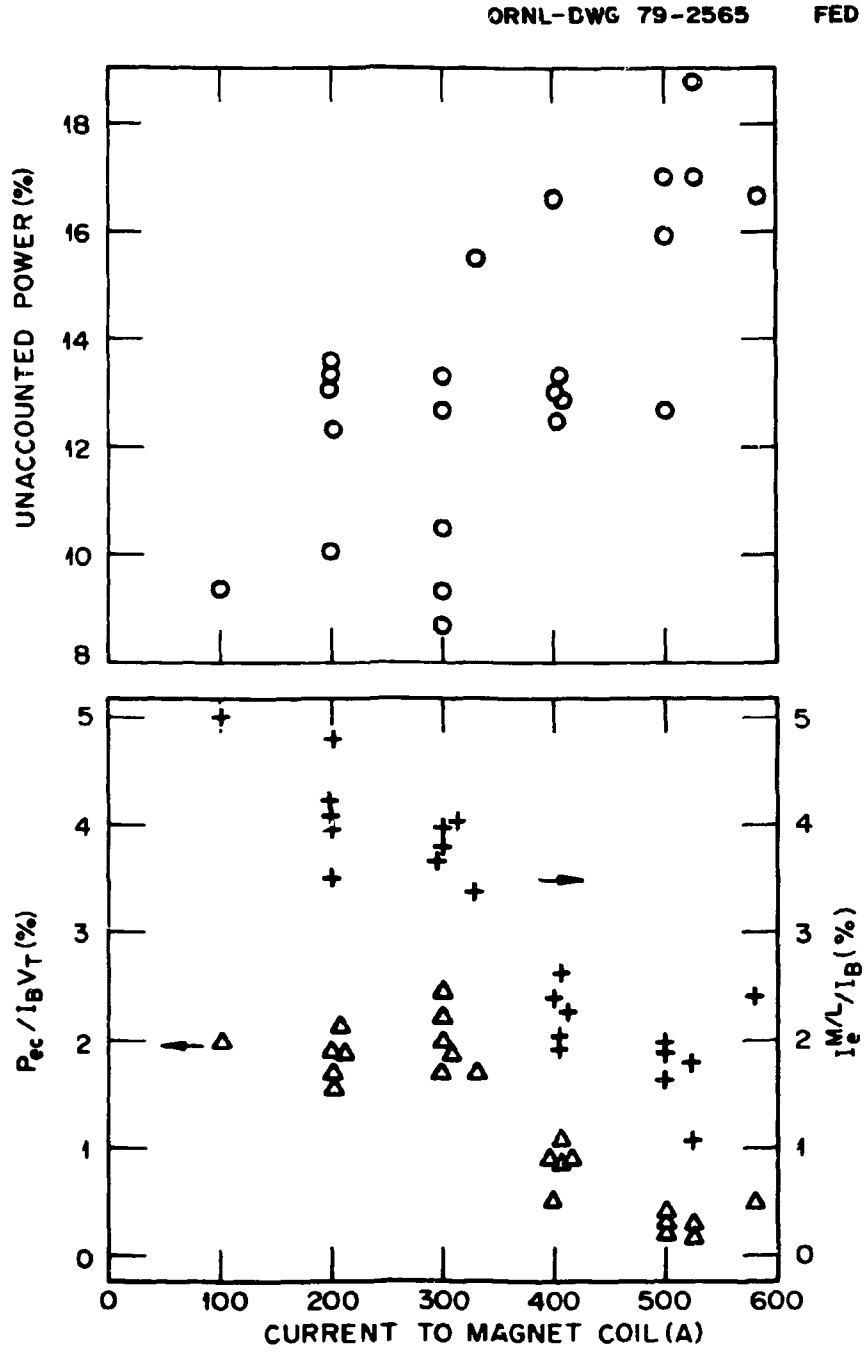

Fig. 4. Deficit in the total calorimetric power in the beam line normalized to I_BV_T (top) and normalized powers on the electron collector and on the magnet pole (bottom), both as a function of the magnetic field strength.

constant level up to a coil current of 300 A, beyond which the level decreases appreciably with increasing magnetic field strength. Power loading to the magnet pole faces, which are at ground potential, is solely due to electrons either (1) leaking out of the gas cell without being effectively suppressed or (2) produced as secondary emissions from the outside wall of the gas cell, resulting from possible ion bombardment. This electron current, deduced from the calorimetric data and the values of V_g, monotonically decreases with increasing magnetic field strength. This variation again appears to be consistent with the variation of the current recovery efficiency shown in Fig. 3.

Figure 5 shows the wave form of I_B and I_D and the corresponding current recovery efficiency as functions of time into a pulse. Also shown is the pressure in the beam line chamber measured downstream from the magnet as a function of time. For a pulse length of 100 ms, the scattered data may indicate that the effectiveness of the recovery scheme is insensitive to pressure and to time into a pulse.

In summary, we note the following features of the present magnetic electron suppression scheme:

1. Electrons in the gas cell seemed to be well suppressed and were found to collect on the electron collector ring by the transverse magnetic field. The level of $\underline{E} \times \underline{B}$ drifted electron current on the ring was low, but was comparable to the recovered ion current. How this electron current will scale with the recovered ion current has yet to be investigated experimentally; however, a theoretical treatment of a similar case has been reported.[10]

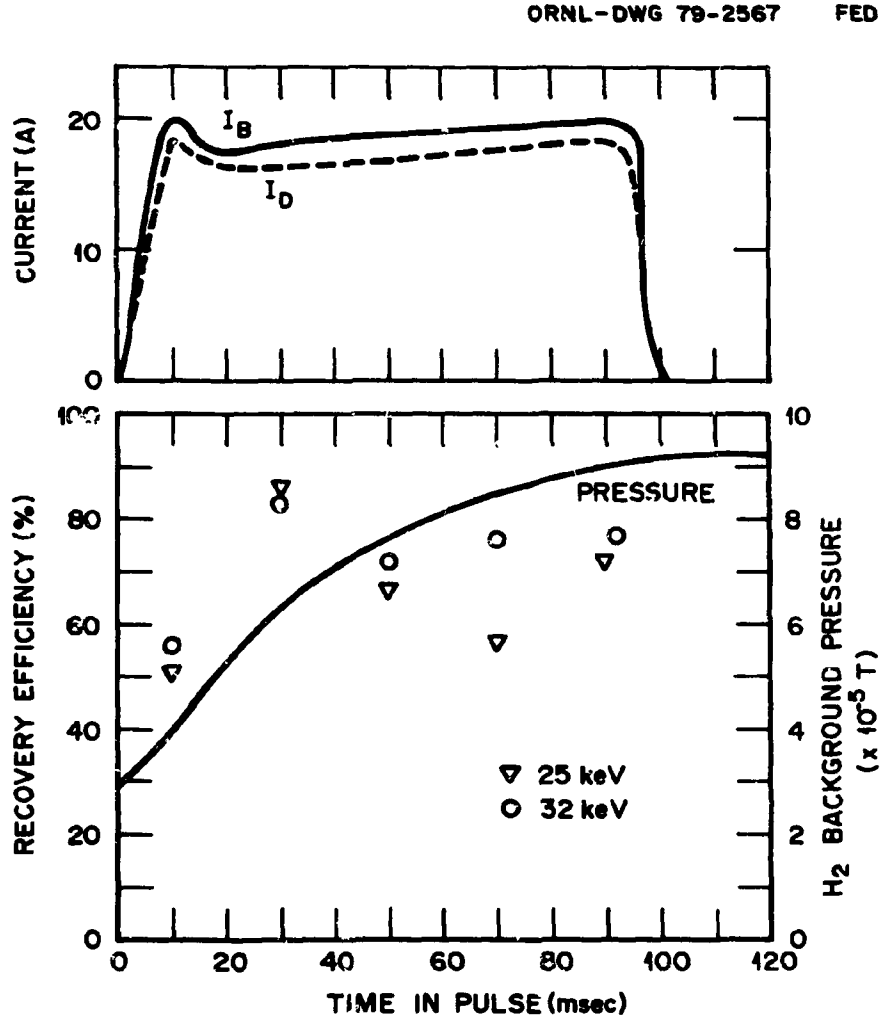

Fig. 5. Time variations of booster and high-voltage power supply (HVPS) drain currents (top) and current recovery efficiency and background pressure (bottom).

2. Handling of lower-energy ions proved to be a very critical factor in achieving a high efficiency because these ions could be the major source of secondary electrons that cannot be suppressed. However, a proper combination of the geometry of the end of the gas cell and the magnetic field strength can confine them within the gas cell and, hence, suppress the secondary electrons. The energy of these ions is not recovered in the present scheme.

3. Unlike the electrostatic suppression scheme, this scheme does *not* necessitate the exposure of any electrodes to the beams, thus eliminating such problems as extra ion loss, secondary emission of electrons, and outgassing.

4. Recovery of full-energy ions is made off the beam axis and hence *does not* rely on space-charge spreading along the beam axis. This fact allows us to provide with ease a large volume and sufficient pumping near the recovery region.

5. This scheme is applicable to any size beam because it does not depend on field penetration or ion space charge, and, in principle, high ion current densities can be handled as well.

4. EXTRAPOLATION TO HIGHER-ENERGY SYSTEMS

Based on the experimental results presented in the preceding section, a conceptual design has been developed in which the fractional-energy ions [H_1^+ (E/2), H_1^+ (E/3), etc.] are *reflected* by a vertical magnet into the gas cell wall and the full-energy ions escape the gas cell–magnet region. A schematic of such a design is illustrated in Fig. 6 for a 120-keV hydrogen injector. Extrapolation to higher energies and to deuterium injectors is rather straightforward. The dimension of the magnet pole, the magnetic field strength, and the geometry of gas cell end structure are the primary parameters to vary in order to make the basic design principle suitable for any extrapolated conditions. The electron collector ring is not shown in Fig. 6. Notice also that the top side of the gas cell is extended for the additional purpose of intercepting negative ions that are present in the beam because of charge-exchange processes.

A parametric study for various beam energies in terms of the system efficiency given by Eq. (3) is shown in Fig. 7. The enhancement factor is defined as $(\eta^R - \eta)/\eta$, where η is the system efficiency *without* recovery and is equal to the numerator of Eq. (2). This is plotted as a function of the energy per nucleon of the beam particle. Curve A represents the "best possible" enhancement that one would obtain by using the recovery scheme, in which the atomic ion fraction (f_1), the transmission efficiency through a gas cell (η_g), and the current recovery efficiency (η_{IR}) are assumed to improve to 90%. Curve B is based on the present technology, where f_1 and η_g are 85% and η_{IR} is 80%. For example, the efficiency of a 160-keV deuterium injector would be enhanced

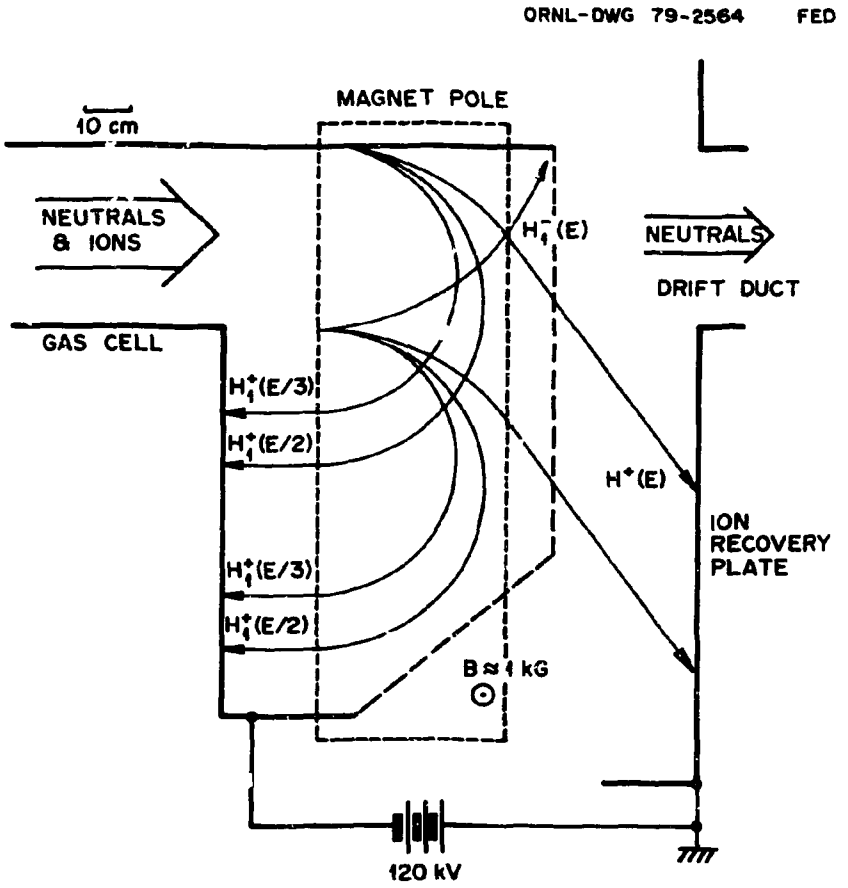

Fig. 6. A conceptual design of a recovery system for 120-keV hydrogen beams 40 cm wide.

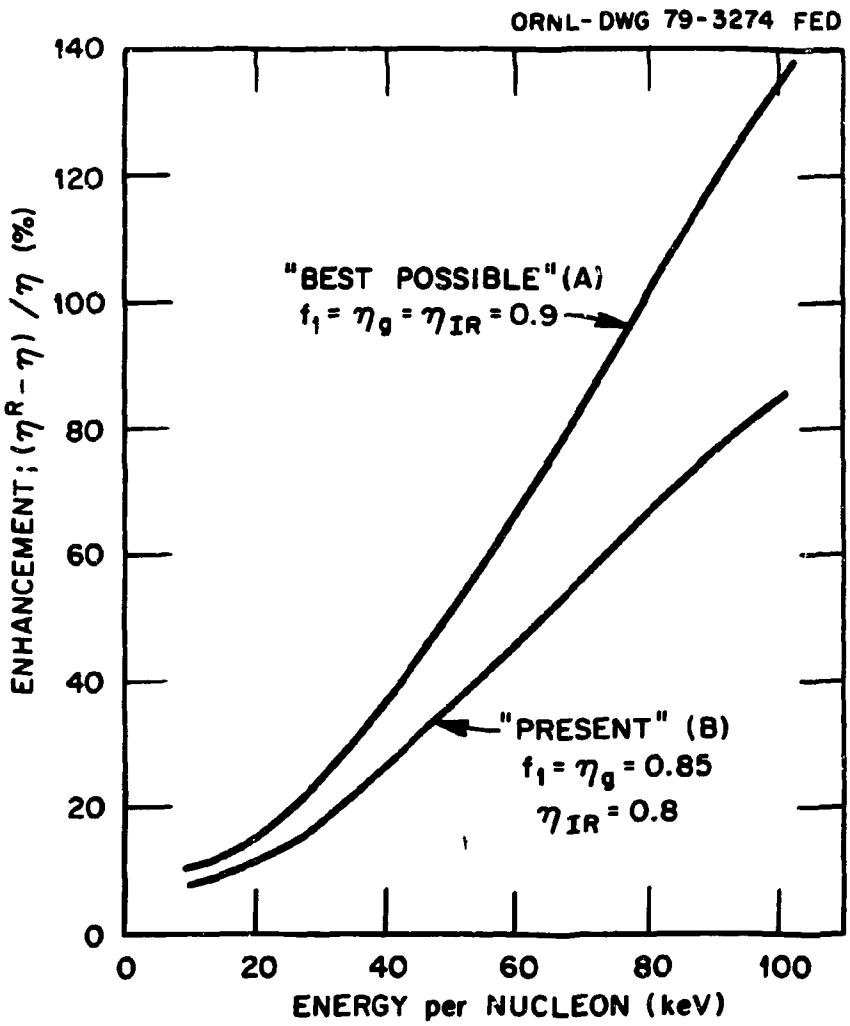

Fig. 7. System efficiency enhancement owing to ion recovery vs nonrecovery as a function of beam energy.

by 65% based on the present technology and by 100% based on the improved technology as a result of the ion energy recovery. It is expected that the enhancement factor increases as the beam energy increases because the ion-to-neutral conversion efficiency (f_o^∞) decreases with the increasing energy.

Values of actual system efficiencies are plotted for the cases of interest in Fig. 8. The equilibrium neutral fraction f_o^∞ is the maximum limit for the system efficiency without recovery in which case the power transmission efficiency to the target (η_t) is 100%. The present technology achieves $\eta_t \cong 60\%$ in the ISX-B neutral beam system.[9] Thus, the curve η is the system efficiency without the ion recovery based on $\eta = 0.6\ f_o^\infty$. The system efficiencies *with* ion energy recovery are shown by the solid lines enhanced by two different cases (A and B of Fig. 7) over the extrapolated efficiency without the recovery η. For a 160-keV deuterium injector, for example, if $\eta_t = 60\%$ is maintained, the system efficiency ($\eta \cong 17\%$ without the recovery) is enhanced to ≈28% with the present parameters and ≈35% with the best possible parameters. Shown also in Fig. 8 is the best possible efficiency in the limit of $\eta_t \to 100\%$ [the curve $f_o^\infty(1 + A)$]. If the enhancement factor at high energies is to remain high (∿100%), the most important remaining parameter will be the power transmission efficiency to a target η_t, which depends on beam optics in a given beam line geometry.

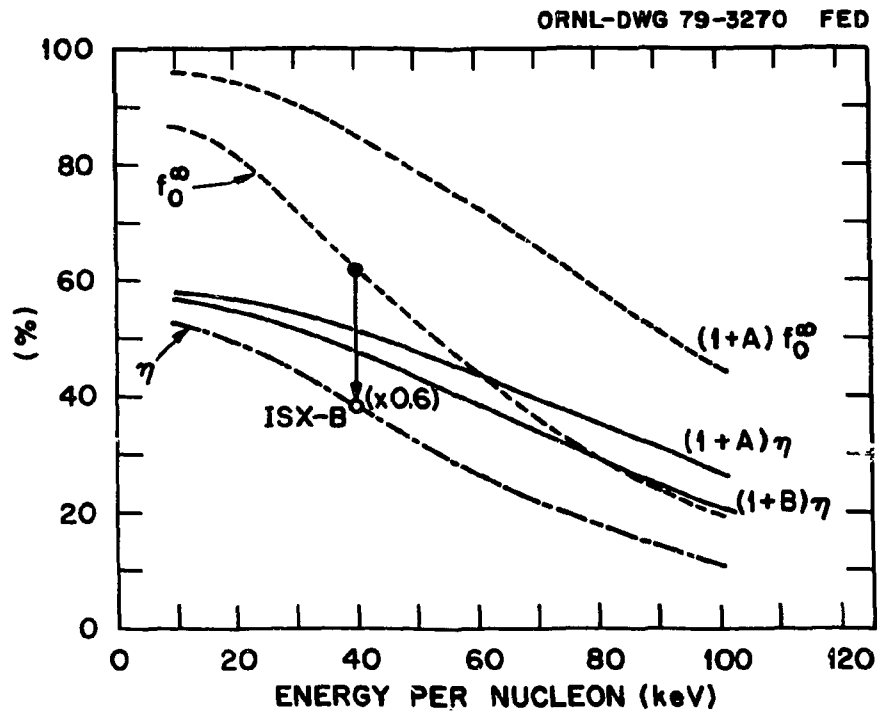

Fig. 8. Actual system efficiencies of various cases as a function of beam energy.

ACKNOWLEDGMENT

We would like to acknowledge the valuable support of our colleagues within the Plasma Technology Section of the Fusion Energy Division.

REFERENCES

1. R. F. Post, *Proc. of the British Nuclear Energy Society Conference on Nuclear Fusion Reactors* (UKAEA, 1970), p. 88-111.
2. R. W. Moir and W. L. Barr, Nucl. Fusion 13, 35 (1973).
3. W. L. Barr and R. W. Moir, *Proc. of the Second Topical Meeting on Technology of Controlled Nuclear Fusion* (American Nuclear Society, 1976), Vol. 4, p. 1181.
4. W. L. Barr, J. N. Doggett, G. W. Hamilton, J. D. Kinney, and R. W. Moir, *Proc. of the Seventh Symposium on Engineering Problems of Fusion Research* (IEEE, 1978), Vol. 1, p. 308.
5. Ph. Raimbault, Report EUR-CEA-FC-823 (1976).
6. Ph. Raimbault, Report EUR-CEA-FC-899 (1977).
7. W. L. Stirling, J. Kim, H. H. Haselton, G. C. Barber, R. C. Davis, W. K. Dagenhart, W. L. Gardner, N. S. Ponte, C. C. Tsai, J. H. Whealton, and R. E. Wright, Appl. Phys. Lett. 35, 104 (1979).
8. R. W. Moir, Lawrence Livermore Laboratory, private communication (1975).
9. J. Kim, W. L. Stirling, M. M. Menon, W. K. Dagenhart, G. C. Barber, R. C. Davis, H. H. Haselton, D. E. Schechter, and C. C. Tsai, Oak Ridge National Laboratory Report ORNL/TM-6896 (1979); in press for J. Appl. Phys.
10. A. T. Forrester, J. Appl. Phys. 46, 2051 (1977).

ORNL/TM-7283
Dist. Category UC-20

INTERNAL DISTRIBUTION

1. G. C. Barber
2. S. C. Bates
3. W. R. Becraft
4. W. K. Dagenhart
5. R. A. Dory
6. P. H. Edmonds
7. R. R. Feezell
8. W. L. Gardner
9. H. H. Haselton
10. W. A. Houlberg
11. T. C. Jernigan
12-16. J. Kim
17. M. M. Menon
18. N. S. Ponte
19. J. A. Rome
20. P. M. Ryan
21. D. E. Schechter
22. J. Sheffield
23. D. Steiner
24-28. W. L. Stirling
29. C. C. Tsai
30. J. H. Whealton
31-32. Central Research Library
33. Document Reference Section
34-35. Laboratory Records
36. Laboratory Records, ORNL-RC
37. ORNL Patent Office
38-39. Fusion Energy Division Library Library
40. Fusion Energy Division Communications Center

EXTERNAL DISTRIBUTION

41. C. C. Baker, Argonne National Laboratory, 9700 South Cass Avenue, Argonne, IL 60439
42. W. L. Barr, Lawrence Livermore Laboratory, University of California, Livermore, CA 94720
43. J. W. Beal, General Atomic Company, P.O. Box 81608, San Diego, CA 92138
44. K. H. Berkner, Lawrence Berkeley Laboratory, University of California, Berkeley, CA 94720
45. Director, Centre d'Etudes Nucleaires, B.P. No. 6, Fontenay-aux-Roses, France
46. J. F. Clarke, Office of Fusion Energy, Department of Energy, Washington, DC 20545
47. F. Coffman, Office of Fusion Energy, Department of Energy, Washington, DC 20545
48. A. Colleraine, General Atomic Company, P.O. Box 81608, San Diego, CA 92138
49. J. R. Conrad, University of Wisconsin, Department of Nuclear Engineering, Madison, WI 53706
50. H. P. Eubank, Plasma Physics Laboratory, Princeton University, P.O. Box 451, Princeton, NJ 08544
51. A. T. Forrester, University of California, Los Angeles, CA 90024
52. T. K. Fowler, Lawrence Livermore Laboratory, University of California, P.O. Box 808, Livermore, CA 94551
53. M. Fumelli, Association Euratom-C.E.A., 92260 Fontenay-aux-Roses, France

54. G. W. Hamilton, Lawrence Livermore Laboratory, University of California, Livermore, CA 94720
55. H. P. Furth, Plasma Physics Laboratory, Princeton University, P.O. Box 451, Princeton, NJ 08544
56. M. Gottlieb, Plasma Physics Laboratory, Princeton University, P.O. Box 451, Princeton, NJ 08544
57. T. S. Green, Culham Laboratory, Abingdon, Oxfordshire, United Kingdom
58. R. Huse, Chairman, EPRI Fusion Program Committee, Public Service Electric and Gas Company, 80 Park Place, Newark, NJ 07101
59. E. E. Kintner, Office of Fusion Energy, Department of Energy, Washington, DC 20545
60. S. Matsuda, Japan Atomic Energy Research Institute, Tokai, Ibaraki, Japan
61. C. N. Meixner, Institut für Plasmaphysik der Kernforschungsanlage, Jülich GmbH, West Germany
62. R. W. Moir, Lawrence Livermore Laboratory, University of California, P.O. Box 808, Livermore, CA 94551
63. Library, Max Planck Institut für Plasmaphysik, Garching bei Munchen, FRG
64. G. H. Miley, Nuclear Engineering Program, University of Illinois, Urbana, IL 61801
65. T. Ohkawa, General Atomic Company, P.O. Box 81608, San Diego, CA 92138
66. Library, Plasma Physics Laboratory, Princeton University, P.O. Box 451, Princeton, NJ 08540
67. R. V. Pyle, Lawrence Berkeley Laboratory, University of California, Berkeley, CA 94720
68. Ph. Raimbault, Association Euratom-C.E.A., 92260 Fontenay-aux-Roses, France
69. G. Schilling, Plasma Physics Laboratory, Princeton University, P.O. Box 451, Princeton, NJ 08544
70. N. N. Semasko, Kurchatov Atomic Energy Institute, Moscow, U.S.S.R.
71. T. Sluyters, Brookhaven National Laboratory, Upton, Long Island, NY 11973
72. E. Speth, Max Planck Institut für Plasmaphysik, Garching bei München, West Germany
73. H. S. Staten, Office of Fusion Energy, Department of Energy, Washington, DC 20545
74. L. D. Stewart, Plasma Physics Laboratory, Princeton University, P.O. Box 451, Princeton, NJ 08544
75. D. R. Sweetman, Culham Laboratory, Abingdon, Oxfordshire, United Kingdom
76. K. Takayama, Director, Institute of Plasma Physics, Nagoya University, Nagoya, Japan
77. E. Thompson, Culham Laboratory, Abingdon, Oxfordshire, United Kingdom
78. F. Valcx, Centre d'Etudes Nucleaires, B.P. No. 6, Fontenay-aux-Roses, France
79. K. Yoshikaw, Institute of Atomic Energy, Kyoto University, Uzi, Kyoto, 611, Japan

80. Office of Assistant Manager, Energy Research and Development, Department of Energy, Oak Ridge Operations, P.O. Box E, Oak Ridge, TN 37830

81-197. Given distribution as shown in TID-4500, Magnetic Fusion Energy (Distribution Category UC-20)